 Bull. Chem. Soc. Jpn. Vol. 86, No. 7, 839–849 (2013)

Synthesis and Characterization of Oxygen/Sulfur-Bridged Incomplete Cubane-Type Clusters, $[M_3S_4(Tpe)_3]^+$ and $[M_3OS_3(Tpe)_3]^+$ (M = Mo and W), and a Mixed-Metal Cubane-Type Cluster, $[Mo_3PdS_4Cl(Tpe)_3]$

Ryouichi Yoshida,[1] Takashi Shibahara,[2] and Haruo Akashi*[1]

[1]Research Institute for Natural Sciences, Okayama University of Science, Ridai-cho, Kita-ku, Okayama 700-0005

[2]Department of Chemistry, Okayama University of Science, Ridai-cho, Kita-ku, Okayama 700-0005

Received December 2, 2012; E-mail: akashi@rins.ous.ac.jp

The reaction of $[Mo_3S_4(H_2O)_9]^{4+}$ (**1**) and $[Mo_3OS_3(H_2O)_9]^{4+}$ (**2**) with hydrotris(pyrazolyl)ethanol (HTpe) ligands produced $[Mo_3S_4(Tpe)_3]PF_6\cdot 3CH_2Cl_2$ ([**5**]$PF_6\cdot 3CH_2Cl_2$) and $[Mo_3OS_3(Tpe)_3]PF_6\cdot 4CH_2Cl_2$ ([**6**]$PF_6\cdot 4CH_2Cl_2$), respectively, using solvent extraction. Furthermore, the tungsten analogous compounds, $[W_3S_4(Tpe)_3]PF_6\cdot 4CH_2Cl_2$ ([**7**]$PF_6\cdot 4CH_2Cl_2$) and $[W_3OS_3(Tpe)_3]PF_6\cdot 2.5CH_2Cl_2$ ([**8**]$PF_6\cdot 2.5CH_2Cl_2$) have been prepared using a similar procedure to that used in the preparation of **5**. The cyclic voltammograms of **5**, **6**, and **7** show one reversible one-electron oxidation process and one reversible one-electron reduction process (**5**, $E_{1/2} = -0.96$ and 1.10 V; **6**, $E_{1/2} = -0.96$ and 1.00 V; **7**, $E_{1/2} = -1.54$ and 0.77 V: all values are given vs. SHE). Complex **8** also shows one reversible ($E_{1/2} = 0.61$ V) and one irreversible one-electron oxidation processes ($E_{pc} = 1.12$ V) and one irreversible one-electron reduction process ($E_{pc} = -1.54$ V). The reaction of **5** with organometallic compound $[Pd_2(dba)_3]$ in CH_3CN afforded $[Mo_3PdS_4Cl(Tpe)_3]\cdot 4.5CH_2Cl_2$ ([**11**]$\cdot 4.5CH_2Cl_2$). Complex **11** showed a high catalytic activity for the intramolecular cyclization of 4-pentynoic acid to give γ-methylene-γ-butyrolactone in the presence of Et_3N. X-ray structure analyses of [**5**]$PF_6\cdot 3CH_2Cl_2$, [**6**]$PF_6\cdot 4CH_2Cl_2$, [**7**]$PF_6\cdot 4CH_2Cl_2$, [**8**]$PF_6\cdot 2.5CH_2Cl_2$, and [**11**]$\cdot 4.5CH_2Cl_2$ revealed that each molybdenum or tungsten atom is bonded to the Tpe ligand.

Mononuclear and dinuclear metal complexes with polypyrazolylborate ligands have been described for ca. 70 metal elements in the periodic table, and much literature has appeared on the complexes, describing the synthesis and application of the compounds in various areas of chemistry.[1,2] However, only a few attempts have been made to study clusters with ligands having three or more metal centers.[3]

We have recently reported that the reactions of $[Mo_3S_4(H_2O)_9]^{4+}$ (**1**)[4] and $[Mo_3OS_3(H_2O)_9]^{4+}$ (**2**)[5] with hindered hydrotris(pyrazolyl)borate (= Tp)[6] ligands afford $[Mo_3S_4(Tp)_3]Cl\cdot 4H_2O$ ([**9**]$Cl\cdot 4H_2O$) and $[Mo_3OS_3(Tp)_3]PF_6\cdot H_2O$ ([**10**]$PF_6\cdot H_2O$), respectively.[7a] These compounds are highly soluble and stable in common organic solvents. The unique redox properties of **9** and **10** have also been reported.[7a] We have also reported that the metal incorporation reactions of **9** afford mixed-metal cubane-type clusters containing Mo_3MS_4 (M = Fe and Ni) cores, and the following compounds, $[Mo_3FeS_4X(Tp)_3]\cdot 4.5CH_2Cl_2$ (X = Cl and Br) and $[Mo_3NiS_4Cl(Tp)_3]\cdot 4CH_2Cl_2$[7c] were successfully isolated from the reactions of **9** with metallic iron or the organo–nickel compound, $[Ni(cod)_2]$ (cod: 1,5-cyclooctadiene).

In this paper, $[Mo_3S_4(Tpe)_3]^+$ (**5**), $[Mo_3OS_3(Tpe)_3]^+$ (**6**), $[W_3S_4(Tpe)_3]^+$ (**7**), and $[W_3OS_3(Tpe)_3]^+$ (**8**) have been successfully isolated from the reactions of M_3S_4 and M_3OS_3 (M = Mo and W) aqua clusters with hydrotris(pyrazolyl)ethanol (= HTpe),[8] respectively (Scheme 1).

$[Mo_3PdS_4Cl(Tpe)_3]$ (**11**) has also been isolated from the reactions of **5** with $[Pd_2(dba)_3]$ (dba: tris(dibenzylidenacetone)dipalladium(0)).

The syntheses and characterizations (X-ray structure analyses, ^1H NMR spectroscopy, X-ray photoelectron spectroscopy, cyclic voltammetry, and catalytic activity) will be discussed.

Experimental

Syntheses. All the following crystalline compounds are efflorescent and the elemental analyses were done after drying under vacuum (overnight). The numbers of solvents before drying were determined by X-ray crystallography.

$[Mo_3S_4(Tpe)_3]PF_6\cdot 3CH_2Cl_2$ ([5]$PF_6\cdot 3CH_2Cl_2$). KPF_6 (155 mg, 0.84 mmol) was added to a green solution of $[Mo_3S_4(H_2O)_9]^{4+}$ (**1**) (in 0.1 M HCl, 5.6×10^{-3} M per trimer, 50 mL). A dichloromethane solution (250 mL) containing tris(1-pyrazolyl)ethanol (= HTpe, 1026 mg, 4.2 mmol) was added to the solution and stirred for two days in air. The organic layer was separated and the solvent was removed under vacuum. The green residue was washed with Et_2O (200 mL) to remove unreacted HTpe. The green powder was recrystallized from dichloromethane (100 mL) to obtain a crystalline product of $[Mo_3S_4(Tpe)_3]PF_6\cdot 3CH_2Cl_2$ ([**5**]$PF_6\cdot 3CH_2Cl_2$). Yield: 288 mg, (80%). Anal. Calcd for [**5**]$PF_6\cdot 0.5CH_2Cl_2$ ($C_{34}H_{34}N_{18}ClO_3Mo_3S_4PF_6$): C, 30.49; H, 2.57; N, 18.83%. Found: C, 30.18; H, 2.32; N, 18.90%. ^1H NMR (CD_3CN, 298 K): δ 5.21 (d, 3H,

Published on the web April 27, 2013; doi:10.1246/bcsj.20120329

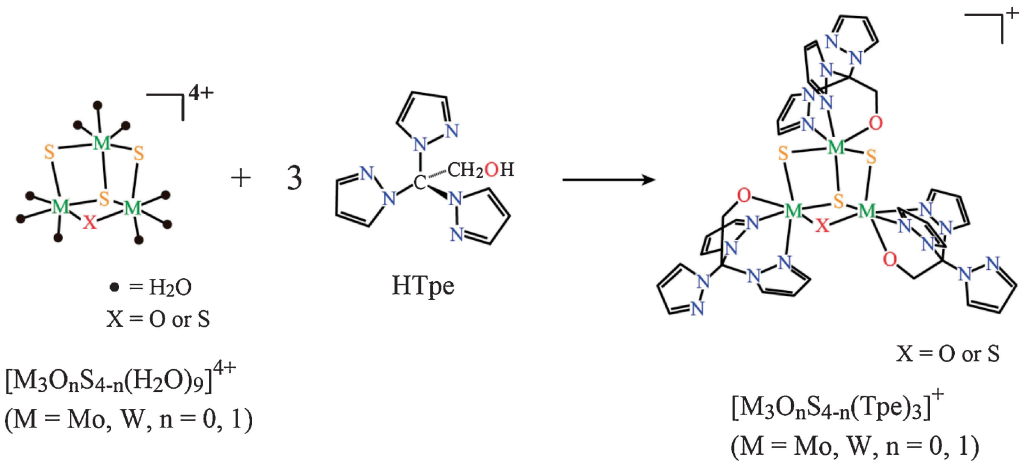

Scheme 1. Preparation scheme of $[M_3O_nS_{4-n}(Tpe)_3]^+$ (M = Mo and W, $n = 0$, 1).

$J = 9.7$ Hz), 5.38 (d, 3H, $J = 9.7$ Hz), 6.37 (t, 3H, $J = 2.5$ Hz), 6.83 (t, 3H, $J = 2.5$ Hz), 6.89 (t, 3H, $J = 2.3$ Hz), 7.49 (d, 3H, $J = 2.8$ Hz), 7.60 (d, 3H, $J = 2.5$ Hz), 8.22 (d, 3H, $J = 2.1$ Hz), 8.35 (d, 3H, $J = 2.5$ Hz), 8.44 (d, 3H, $J = 2.1$ Hz), 8.66 (d, 3H, $J = 2.1$ Hz).

The following compounds (except **11**) were prepared by a similar procedure to that used in the preparation of complex **5**.

$[Mo_3OS_3(Tpe)_3]PF_6\cdot 4CH_2Cl_2$ ([6]$PF_6\cdot 4CH_2Cl_2$). KPF_6 (155 mg, 0.84 mmol) was added to a green solution of $[Mo_3OS_3(H_2O)_9]^{4+}$ (**2**) (in 0.1 M HCl, 6.6×10^{-3} M per trimer, 50 mL). A dichloromethane solution (250 mL) containing HTpe (1209 mg, 4.95 mmol) was added to the solution and stirred for two days. The organic layer was separated and solvent was removed under vacuum. The green residue was washed by Et_2O (200 mL) to remove unreacted HTpe. The green powder was recrystallized from dichloromethane to obtain a crystalline product of $[Mo_3OS_3(Tpe)_3]PF_6\cdot 4CH_2Cl_2$ ([**6**]$PF_6\cdot 4CH_2Cl_2$). Yield: 290 mg, (69%). Anal. Calcd for [**6**]PF_6 ($C_{33}H_{33}N_{18}O_4Mo_3S_3PF_6$): C, 31.09; H, 2.61; N, 19.78%. Found: C, 31.17; H, 2.60; N, 19.57%. ^{1}H NMR (CD_2Cl_2, 298 K): δ 5.15 (d, 1H, $J = 9.6$ Hz), 5.32 (d, 1H, $J = 9.6$ Hz), 5.32 (d, 1H, $J = 9.6$ Hz), 5.40 (d, 1H, $J = 9.6$ Hz), 5.45 (d, 1H, $J = 9.6$ Hz), 5.50 (d, 1H, $J = 9.6$ Hz), 6.31 (t, 1H, $J = 2.5$ Hz), 6.32 (t, 1H, $J = 2.5$ Hz), 6.38 (t, 1H, $J = 2.5$ Hz), 6.67 (t, 1H, $J = 2.5$ Hz), 6.70 (t, 1H, $J = 2.5$ Hz), 6.75 (t, 1H, $J = 2.5$ Hz), 6.82 (t, 1H, $J = 2.5$ Hz), 6.83 (t, 1H, $J = 2.5$ Hz), 6.84 (t, 1H, $J = 2.5$ Hz), 7.35 (d, 1H, $J = 2.5$ Hz), 7.42 (d, 1H, $J = 3.0$ Hz), 7.45 (d, 1H, $J = 3.0$ Hz), 7.47 (d, 1H, $J = 3.0$ Hz), 7.48 (d, 1H, $J = 3.0$ Hz), 7.55 (d, 1H, $J = 2.7$ Hz), 8.07 (br s, 1H), 8.10 (d, 1H, $J = 2.1$ Hz), 8.12 (d, 1H $J = 2.2$ Hz), 8.14 (d, 1H, $J = 2.4$ Hz), 8.15 (d, 1H, $J = 2.4$ Hz), 8.17 (d, 1H, $J = 2.0$ Hz), 8.18 (d, 1H, $J = 2.0$ Hz), 8.18 (d, 1H, $J = 2.0$ Hz), 8.20 (d, 1H, $J = 3.0$ Hz), 8.32 (d, 1H, $J = 2.1$ Hz), 8.73 (d, 1H, $J = 2.1$ Hz), 8.84 (br s, 1H).

$[W_3S_4(Tpe)_3]PF_6\cdot 4CH_2Cl_2$ ([7]$PF_6\cdot 4CH_2Cl_2$). KPF_6 (105 mg, 0.57 mmol) was added into a purple solution of $[W_3S_4(H_2O)_9]^{4+}$ (**3**)[9] (in 0.1 M HCl, 7.6×10^{-3} M per trimer, 25 mL). A dichloromethane solution (150 mL) containing HTpe (696 mg, 2.85 mmol) was added to the solution and stirred two days. The organic layer was separated and solvent was removed under vacuum. The purple residue was washed by Et_2O (200 mL) to remove unreacted HTpe. The purple powder was recrystallized from dichloromethane (100 mL) to obtain a crystalline product of $[W_3S_4(Tpe)_3]PF_6\cdot 4CH_2Cl_2$ ([**7**]$PF_6\cdot 4CH_2Cl_2$). Yield: 30 mg, (10%). Anal. Calcd for [**7**]$PF_6\cdot 0.5CH_2Cl_2$ ($C_{34}H_{34}N_{18}ClO_3S_4PF_6W_3$): C, 25.20; H, 2.15; N, 15.79%. Found: C, 25.28; H, 1.93; N, 15.78%. ^{1}H NMR (CD_3CN, 298 K): δ 5.12 (d, 3H, $J = 9.8$ Hz), 5.51 (d, 3H, $J = 9.8$ Hz), 6.41 (t, 3H, $J = 2.5$ Hz), 6.84 (t, 3H, $J = 2.5$ Hz), 6.89 (t, 3H, $J = 2.3$ Hz), 7.44 (d, 3H, $J = 2.4$ Hz), 7.58 (d, 3H, $J = 2.8$ Hz), 8.21 (d, 3H, $J = 1.9$ Hz), 8.33 (d, 3H, $J = 2.5$ Hz), 8.75 (t, 6H, $J = 3.3$ Hz).

$[W_3OS_3(Tpe)_3]PF_6\cdot 2.5CH_2Cl_2$ ([8]$PF_6\cdot 2.5CH_2Cl_2$). KPF_6 (110 mg, 0.6 mmol) was added to a purple solution of $[W_3OS_3(H_2O)_9]^{4+}$ (**4**)[10] (in 0.1 M HCl, 8.0×10^{-3} M per trimer, 25 mL). A dichloromethane solution (150 mL) containing HTpe (733 mg, 3.0 mmol) was added to the solution and stirred for two days. The organic layer was separated and solvent was removed under vacuum. The purple residue was washed by Et_2O (200 mL) to remove unreacted HTpe. The purple powder was recrystallized from dichloromethane (100 mL) to obtain a crystalline product of $[W_3OS_3(Tpe)_3]PF_6\cdot 2.5CH_2Cl_2$ ([**8**]$PF_6\cdot 2.5CH_2Cl_2$). Yield: 132 mg, (43%). Anal. Calcd for [**8**]PF_6 ($C_{33}H_{33}N_{18}O_4W_3S_3PF_6$): C, 25.76; H, 2.16; N, 16.39%. Found: C, 25.75; H, 1.90; N, 16.13%. ^{1}H NMR (CD_2Cl_2, 298 K): δ 5.09 (d, 1H, $J = 9.6$ Hz), 5.22 (d, 1H, $J = 9.6$ Hz), 5.29 (d, 1H, $J = 9.6$ Hz), 5.41 (d, 1H, $J = 9.6$ Hz), 5.53 (d, 1H, $J = 9.6$ Hz), 5.60 (d, 1H, $J = 9.6$ Hz), 6.34 (t, 1H, $J = 2.5$ Hz), 6.35 (t, 1H, $J = 2.5$ Hz), 6.41 (t, 1H, $J = 2.5$ Hz), 6.68 (t, 1H, $J = 2.5$ Hz), 6.71 (t, 1H, $J = 2.5$ Hz), 6.75 (t, 1H, $J = 2.5$ Hz), 6.82 (t, 1H, $J = 2.0$ Hz), 6.83 (t, 1H, $J = 2.0$ Hz), 6.84 (t, 1H, $J = 2.0$ Hz), 7.30 (d, 1H, $J = 2.8$ Hz), 7.38 (d, 1H, $J = 2.8$ Hz), 7.41 (d, 1H, $J = 2.8$ Hz), 7.42 (d, 1H, $J = 2.8$ Hz), 7.46 (d, 1H, $J = 2.8$ Hz), 7.53 (d, 1H, $J = 2.8$ Hz), 8.10 (br s, 1H), 8.12 (d, 1H, $J = 2.8$ Hz), 8.13 (br s, 1H), 8.15 (br s, 1H), 8.16 (d, 1H, $J = 2.8$ Hz), 8.16 (d, 1H, $J = 2.8$ Hz), 8.18 (d, 1H, $J = 2.1$ Hz), 8.18 (d, 1H, $J = 2.1$ Hz), 8.36 (d, 1H, $J = 2.1$ Hz), 8.59 (d, 1H, $J = 2.0$ Hz), 8.89 (d, 1H, $J = 2.0$ Hz), 9.10 (br s, 1H).

$[Mo_3PdS_4Cl(Tpe)_3]\cdot 4.5CH_2Cl_2$ ([11]$\cdot 4.5CH_2Cl_2$). This compound was prepared under an N_2 atmosphere. Cluster [**5**]$PF_6\cdot 3CH_2Cl_2$ (100 mg, 0.078 mmol) was dissolved in acetonitrile (40 mL). $[Pd_2(dba)_3]$ (71 mg, 0.078 mmol) and bis-(triphenylphosphoranylidene)ammonium chloride (=PPNCl,

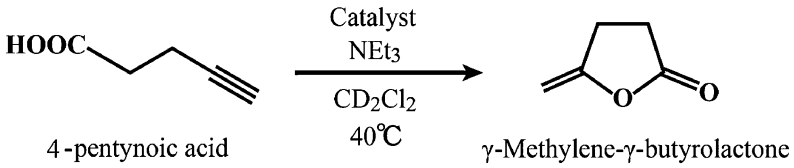

Scheme 2. Catalytic intramolecular cyclization of 4-pentynoic acid.

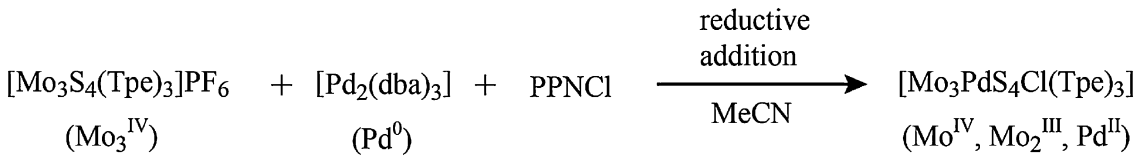

Scheme 3. Reaction scheme of **5** with $[Pd_2(dba)_3]$.

54 mg, 0.094 mmol) were added to the green solution and stirred 3 days. Black-purple powder of **11** and palladium powder deposited during stirring. The precipitates were collected by filtration and washed with dichloromethane to separate the palladium powder. The filtrate was kept in a refrigerator for three days to give black-purple crystals of $[Mo_3PdS_4Cl(Tpe)_3]\cdot 4.5CH_2Cl_2$ ([**11**]·$4.5CH_2Cl_2$). Yield: 60 mg, (56%). Anal. Calcd for [**11**]·CH_2Cl_2 ($C_{34}H_{35}Cl_3Mo_3N_{18}O_3PdS_4$): C, 29.75; H, 2.57; N, 18.37%. Found: C, 29.59; H, 2.41; N, 18.69%. ^{1}H NMR (CD_2Cl_2, 298 K): δ 5.04 (d, 3H, $J = 9.1$ Hz), 5.30 (d, 3H, $J = 9.1$ Hz), 6.33 (t, 3H, $J = 2.5$ Hz), 6.42 (t, 3H, $J = 2.5$ Hz), 6.75 (t, 3H, $J = 2.3$ Hz), 7.04 (d, 3H, $J = 2.9$ Hz), 7.49 (d, 3H, $J = 2.7$ Hz), 8.09 (s, 6H), 8.26 (d, 3H, $J = 2.2$ Hz), 9.34 (s, 3H).

X-ray Crystallography. Each of the crystals of [**5**]$PF_6\cdot 3CH_2Cl_2$, [**6**]$PF_6\cdot 4CH_2Cl_2$, [**7**]$PF_6\cdot 4CH_2Cl_2$, [**8**]$PF_6\cdot 2.5CH_2Cl_2$, and [**11**]·$4.5CH_2Cl_2$ suitable for the X-ray crystallography was covered with paraton-N and mounted in a Micro mesh (Hampton Research Corp.). Data collection was performed (at 93 K) on a Rigaku RAXIS-IV two-dimensional detector equipped with a low-temperature apparatus by use of graphite-monochromated Mo Kα radiation ($\lambda = 0.71073$ Å). Empirical absorption correction using the program was applied.[11] The structures of the compounds were solved by the direct method (SHELX 97[12]) with the aid of successive difference Fourier maps and refined by full-matrix least-squares method on F^2. All hydrogen atoms were included in the refinement at calculated positions, riding on their carrier atoms (C–H 0.95 Å). Isotropic thermal parameters of hydrogen atoms were constrained to 1.2 U_{eq} to which they were attached. The final difference Fourier maps showed no significant electron density. All calculations were performed with the program package Crystal Structure 3.8.2.[13]

Crystallographic data have been deposited with The Cambridge Crystallographic Data Centre: Deposition number CCDC-913305, 913306, 913307, 913308, and 913309 for compounds [**5**]$PF_6\cdot 3CH_2Cl_2$, [**6**]$PF_6\cdot 4CH_2Cl_2$, [**7**]$PF_6\cdot 4CH_2Cl_2$, [**8**]$PF_6\cdot 2.5CH_2Cl_2$, and [**11**]·$4.5CH_2Cl_2$. Copies of the data can be obtained free of charge via www.ccdc.cam.ac.uk/data_request/cif (or from The Cambridge Crystallographic Data Centre, 12, Union Road, Cambridge, CB2 1EZ, UK; e-mail: data_request@ccdc.cam.ac.uk).

Electronic Spectroscopy. The UV–vis absorption spectra were measured on a Hitachi U-2000 spectrophotometer at room temperature.

^{1}H NMR Spectroscopy. The ^{1}H NMR spectra were measured on a Bruker ARX-NMR spectrometer (Temperature, 298 K; Frequency, 400 MHz; Standard, solvent, $CD_3CN = 2.00$ ppm, $CD_2Cl_2 = 5.33$ ppm).

Cyclic Voltammetry. All the measurement procedures were performed under argon atmosphere. Solutions of [**5**]PF_6, [**6**]PF_6, [**7**]PF_6, and [**8**]PF_6 (0.5 mM, in MeCN containing 0.1 M n-Bu_4NPF_6 as supporting electrolyte) were purged with argon gas prior to measurement. Cyclic voltammetry was performed using a BAS 100B/W analyzer (Bio Analytical System Inc.) employing a platinum wire working electrode, a platinum wire auxiliary electrode, and a Ag/Ag^+ (MeCN) reference electrode (0.1 M $AgPF_6$). The potential for the ferrocene/ferrocenium couple ($E_{1/2}$) is observed at 0.084 V under identical conditions.

XPS Spectroscopy. The X-ray photoelectron spectroscopic measurement was performed with a Shimadzu/Kratos AXIS-HS using monochromated aluminum Kα radiation (15 kV, 5 mA) for wide-range measurement and narrow-range measurement (C 1s, Mo 3d, Pd 3d, and S 2p). The standard $C_{1s} = 285.0$ eV was employed. Each of the crystals of [**9**]Cl, [**5**]PF_6, **11**, and $[Mo_3PdS_4Cl(Tp)_3]$ (**12**) was ground to a powder, and the powder sample was mounted on the sample table using a copper plated cloth tape X7001 (Sumitomo 3M LTD). A charge neutralizer was applied to prevent charging of the sample.

Catalytic Reaction. Catalytic activity of **11** has been tested by the intramolecular cyclization reaction of 4-pentynoic acid (Scheme 2). Cluster **11** (4.4 mg) was dissolved in CH_2Cl_2 (100 mL). The solution (0.1 mL) was moved to an NMR sample tube using a gastight Hamilton syringe. After removal of the solvent under vacuum, the residue was redissolved by the addition of CD_2Cl_2 (0.75 mL). 4-Pentynoic acid (294.3 mg, 3 mmol) and NEt_3 (4.5 μL, 0.03 mmol) were added to the solution, and the reaction progress was monitored by ^{1}H NMR spectrometry, and the abundance of 4-pentynoic acid and γ-methylene-γ-butyrolactone was determined by the integrated intensities of the ^{1}H NMR signals of these compounds.

Results and Discussion

Syntheses. [**5**]$PF_6\cdot 3CH_2Cl_2$ was successfully isolated from the reaction of $[Mo_3S_4(H_2O)_9]^{4+}$ (**1**) with HTpe in 80% isolated yield. [**6**]$PF_6\cdot 4CH_2Cl_2$, [**7**]$PF_6\cdot 4CH_2Cl_2$, and [**8**]$PF_6\cdot 2.5CH_2Cl_2$ were prepared using a similar method to that for **5** (Scheme 1). A solvent extraction method was employed in

this preparation method. The deprotonation of the HTpe ligand is important for this reaction. The use of 0.1 M HCl gave **5** in high yield, while the use of 2 M HCl gave little of the target complex. An excessively low acid concentration (ca. 0.01 M) of the aqueous layer leads to the decomposition of **1**. Clusters **5**, **6**, **7**, and **8** are soluble and stable in dichloromethane and acetonitrile.

The addition of $[Pd_2(dba)_3]$ and PPNCl used for the chloride anion source to an acetonitrile solution of [**5**]PF_6 affords a purple microcrystalline solid of the neutral complex $[Mo_3PdS_4Cl(Tpe)_3]\cdot 4.5CH_2Cl_2$ ([**11**]$\cdot 4.5CH_2Cl_2$). Cluster **11** is soluble and stable in dichloromethane and chloroform. This palladium insertion reaction is a reductive addition. The formal oxidation state of molybdenum atoms changed from Mo_3^{IV} to $Mo^{IV}Mo_2^{III}$, and that of palladium atom from Pd^0 to Pd^{II} (Scheme 3, See XPS section).

Cluster **5** reacts with $[Pd_2(dba)_3]$ and functions as a metal-complex ligand for preparing novel mixed-metal complexes even in nonaqueous solvents, while clusters **6**, **7**, and **8** do not react with $[Pd_2(dba)_3]$. As already mentioned in our previous report, Complex **1** and its derivatives are useful platforms to prepare various kinds of cubane-type mixed-metal clusters; we have reported the reactivity of lone pair electrons of μS atoms in **1** and its ability to incorporate heterometals to afford a series of mixed-metal cubane-type sulfide clusters containing Mo_3MS_4 cores (M = Fe,[7] Co,[14] Ni,[15] Cu,[16] Zn,[17] Ga,[18] Cd,[19] In,[20] Sn,[21] Sb,[22] Hg,[14] Sn^{2+},[21] and Cu^{+} [16]). Some papers related to the metal incorporation reaction of **1** or its derivatives have also been published by other researchers.[23] Many examples of the metal incorporation reaction of the complex **1** and a few of **2** have been reported,[24] while the reaction of $[Mo_3O_4(H_2O)_9]^{4+}$ has not been reported. The large reactivity difference between the two clusters $[Mo_3S_4(H_2O)_9]^{4+}$ and $[Mo_3O_4(H_2O)_9]^{4+}$ have been explained by the DV-Xα calculation.[25]

X-ray Crystallography. Crystallographic and refinement data for [**5**]$PF_6\cdot 3CH_2Cl_2$, [**6**]$PF_6\cdot 4CH_2Cl_2$, [**7**]$PF_6\cdot 4CH_2Cl_2$, [**8**]$PF_6\cdot 2.5CH_2Cl_2$, and [**11**]$\cdot 4.5CH_2Cl_2$ are summarized in Table 1. ORTEP drawings of the clusters **5** (and **9**), **6**, **7**, **8**, and **11** are shown in Figures 1–5, respectively.

Clusters **5**, **6**, **7**, and **8** have incomplete cubane-type cores. The general formula of these compounds is $[M_3O_nS_{4-n}(Tpe)_3]^+$ (M = Mo and W, n = 0, 1). All the molybdenum or tungsten atoms bonded to the Tpe ligand. The Tpe ligand acts in a tridentate fashion and coordinated to the molybdenum or tungsten atom through the two nitrogen atoms of the pyrazole rings and the one oxygen atom of the ethoxy group. This coordination mode leads to reduced steric hindrance between the Tpe ligands, as compared with the case of the Tp ligands in [**9**]$Cl\cdot 4H_2O$[7a] (Figure 1). The Tp ligand coordinated to a molybdenum atom through the three nitrogen atoms of pyrazole rings. If Mo–Mo bonds are ignored, each molybdenum atom has a six-coordinated, distorted-octahedral geometry in **9**. Steric hindrance between the ligands Tps may be the cause of the distortion. A projection of the compound **5** down to the C10–Mo1 axis is shown in Figure 1. Tpe ligands coordinated to Mo2 and Mo3 were omitted for clarity. For comparison, a projection of **9** down to the B1–Mo1 axis is also shown in Figure 1, where only the crystallographically independent atoms are shown except Mo1*, S2*, Mo1**, and S2** atoms (symmetry oper-

Table 1. Crystallographic and Refinement Data for [**5**]$PF_6\cdot 3CH_2Cl_2$, [**7**]$PF_6\cdot 4CH_2Cl_2$, [**6**]$PF_6\cdot 4CH_2Cl_2$, [**8**]$PF_6\cdot 2.5CH_2Cl_2$, and [**11**]$\cdot 4.5CH_2Cl_2$

	$[Mo_3S_4(Tpe)_3]PF_6\cdot 3CH_2Cl_2$	$[W_3S_4(Tpe)_3]PF_6\cdot 4CH_2Cl_2$	$[Mo_3OS_3(Tpe)_3]PF_6\cdot 4CH_2Cl_2$	$[W_3OS_3(Tpe)_3]PF_6\cdot 2.5CH_2Cl_2$	$[Mo_3PdS_4Cl(Tpe)_3]\cdot 4.5CH_2Cl_2$
Empirical formula	$C_{36}H_{39}Cl_6F_6Mo_3N_{18}O_3PS_4$	$C_{37}H_{41}Cl_8F_6N_{18}O_3PS_4W_3$	$C_{37}H_{41}Cl_8F_6Mo_3N_{18}O_4PS_3$	$C_{35.5}H_{38}Cl_5F_6N_{18}O_4PS_3W_3$	$C_{37.5}H_{42}Cl_{10}Mo_3N_{18}O_3S_4$
fw	1545.57	1849.75	1617.47	1750.74	1617.47
Cryst syst	monoclinic	monoclinic	monoclinic	monoclinic	Trigonal
a/Å	14.6306(4)	14.4119(2)	14.5248(8)	15.0723(14)	18.457(3)
b/Å	21.8955(5)	21.8031(3)	21.6753(9)	23.8019(17)	
c/Å	19.3600(5)	19.1920(3)	19.1551(8)	17.0045(17)	34.574(6)
β/degree	107.1330(5)	107.6003(6)	107.9988(16)	110.443(2)	
V/Å^3	5926.6(3)	5748.29(14)	5735.5(5)	5716.2(9)	10200(3)
T/K	113	93	93	93	93
Space group	$P2_1/n$ (#14)	$P2_1/n$ (#14)	$P2_1/n$ (#14)	$P2_1/n$ (#14)	$R\bar{3}$ (#148)
Z	4	4	4	4	6
μ(Mo Kα)/cm^{-1}	11.326	65.675	12.308	64.381	13.624
Reflns collected	35807	41171	38470	20667	16825
Unique reflns/R_{int}	12747 (R_{int} = 0.058)	12647 (R_{int} = 0.034)	11220 (R_{int} = 0.034)	9598 (R_{int} = 0.042)	4774 (R_{int} = 0.063)
R; wR_2 (all data)	0.089; 0.192	0.043; 0.081	0.076; 0.182	0.085; 0.224	0.070; 0.203
R_1 ($I > 2.00\sigma(I)$)	0.066	0.036	0.068	0.080	0.061

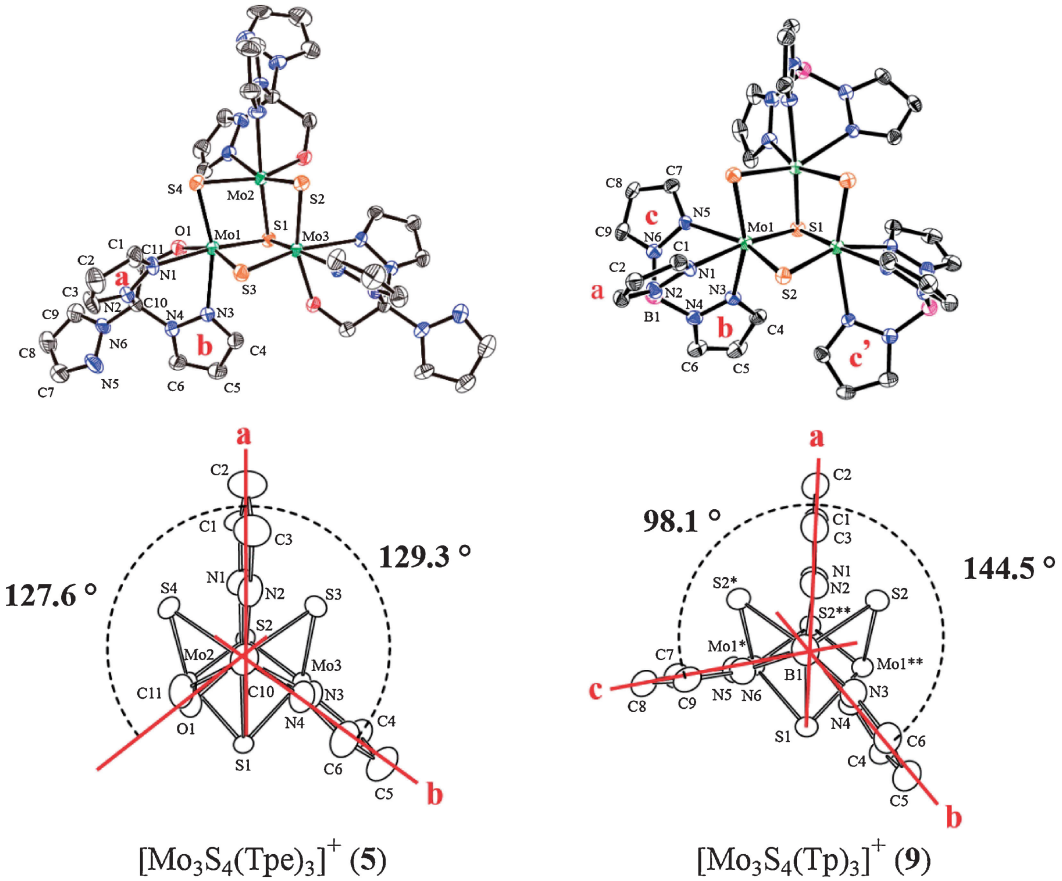

Figure 1. ORTEP drawings of **5** and **9**.

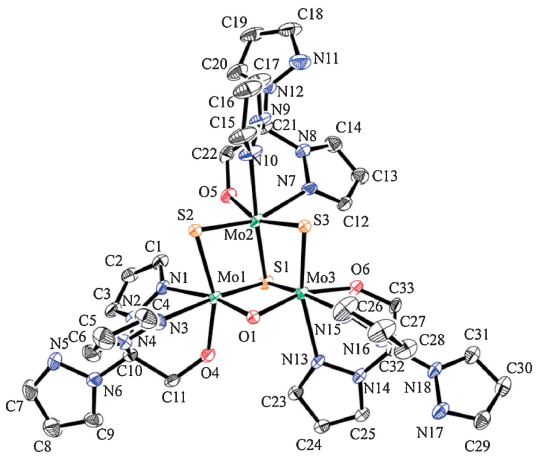

Figure 2. ORTEP drawing of **6**.

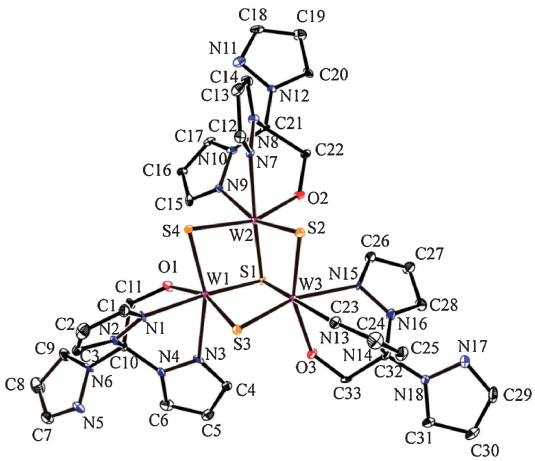

Figure 3. ORTEP drawing of **7**.

ators: * $-x+y, -x, +z$, ** $-y, +x-y, +x$). In the case of **9**, the dihedral angle between the pyrazole rings **a** (N1, N2, C1, C2, C3) and **b** (N3, N4, C4, C5, C6) is 144.5°, whereas the dihedral angle between the pyrazole rings **a** (N1, N2, C1, C2, C3) and **c** (N5, N6, C7, C8, C9) is much smaller: 98.1°. Therefore, the pyrazole ring **b** is under the pyrazole ring **c′** that is coordinated to the adjacent molybdenum atom so that the pyrazole rings **b** and **c′** have less steric hindrance (Figure 1). On the other hand, the dihedral angle between the pyrazole rings **a** (N1, N2, C1, C2, C3) and **b** (N3, N4, C4, C5, C6) is 129.3°, and that between the pyrazole ring **a** (N1, N2, C1, C2, C3) and the basal plane defined by Mo1, O1, C11, C10 is 127.6° in **5**. The reduced steric hindrance of the ethoxy group with respect to the pyrazole ring leads to less distorted octahedral coordination geometry.

The Mo–Mo, Mo–μS, and Mo–μ_3S distances in analogous complexes having $Mo^{IV}_3S_4$ cores are listed in Table 2. The Mo–Mo distances (2.810[8] Å) in **5** are slightly longer than those (2.732[7] Å) in **1**. The elongation of the Mo–Mo distances is probably due to the electron donating ability of Tpe ligands. Similar elongation effects are observed with the

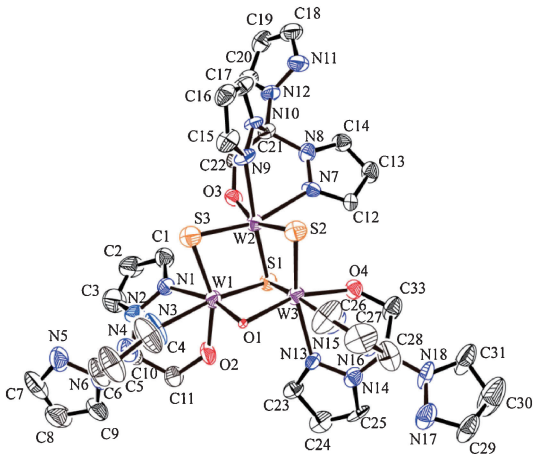

Figure 4. ORTEP drawing of **8**.

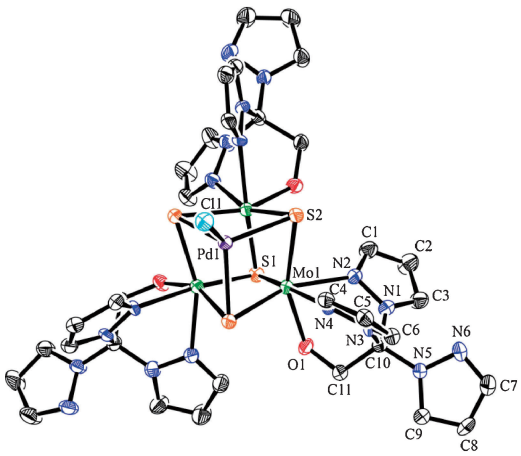

Figure 5. ORTEP drawing of **11**.

Table 2. Comparison of Mo–Mo and Mo–S Distances (Å) in Incomplete Cubane-Type Compounds with $Mo^{IV}{}_3S_4$ Cores[a),b)]

Compound	Mo–Mo	Mo–μ_3S	Mo–μ_2S
$[Mo_3S_4(Tp)_3]Cl\cdot 4H_2O$ ([**9**]Cl·4H$_2$O)[7a]	2.8314(3)	2.3576(8)	2.2689(8)
$[\{Mo_3S_4Tp_2\}_2O(pz)_2]\cdot 2THF$[3a]	2.830[24]	2.352[11]	2.292[22]
$[Mo_3S_4Cp^*{}_3]PF_6$[26]	2.8196[5]	2.3240[11]	2.2957[12]
$[Mo_3S_4Cp_3][Sn(CH_3)_3Cl_2]$[27]	2.812[1]	2.314[6]	2.294[6]
$[Mo_3S_4(Tpe)_3]PF_6\cdot 3CH_2Cl_2$ ([**5**]PF$_6$·3CH$_2$Cl$_2$)	2.810[8]	2.356[6]	2.299[11]
$[Mo_3S_4Cl_4(PEt_3)_4(MeOH)]$[28]	2.790[5]	2.359[8]	2.289[23]
$[(C_2H_5)_4N]_2[Mo_3S_4(SCH_2CH_2S)_3]$[29]	2.783[12]	2.345[3]	2.293[22]
$K_5[Mo_3S_4(CN)_9]\cdot 7H_2O$[30]	2.765[7]	2.363[4]	2.312[5]
$[Mo_3S_4(dtp)_4(H_2O)]$[31]	2.754[18]	2.346[9]	2.281[19]
$Na_2[Mo_3S_4(Hnta)_3]\cdot 5H_2O$[32]	2.754[18]	2.334[4]	2.290[13]
$Ca[Mo_3S_4(ida)_3]\cdot 11.5H_2O$[33]	2.754[11]	2.348[9]	2.294[8]
$[Mo_3S_4(dtc)_4(dmf)]\cdot EtOH$[34]	2.741[38]	2.336[3]	2.297[3]
$Cs[Mo_3S_4(ox)_3(H_2O)_3]\cdot 3H_2O$[35]	2.738(5)	2.33(1)	2.28(1)
$[Mo_3S_4(H_2O)_9](pts)_4\cdot 9H_2O$ ([**1**](pts)$_4$·9H$_2$O)[4]	2.732[7]	2.332[4]	2.286[6]

a) Abbreviations: dtp: $(C_2H_5)_2PS_2$, Hnta: $N(CH_2COO)_3H^{2-}$, ida: $HN(CH_2COO)_2{}^{2-}$, dtc: $(C_2H_5)_2NCS_2{}^-$, ox: $C_2O_4{}^{2-}$. b) Parentheses indicate esd of one value. The estimated deviation in brackets is calculated as being equal to $[\Sigma\Delta_i{}^2/n(n-1)]^{1/2}$, in which Δ_i is deviation of the ith (of n) value from the arithmetic mean of the n values.

Mo–Mo distances in **9**, $[\{Mo_3S_4(Tp)_2\}_2(\mu\text{-}O)(\mu\text{-}pz)_2]\cdot 2THF$,[3a] $[Mo_3Cp^*{}_3S_4]PF_6$ (Cp*: C_5Me_5),[26] and $[Mo_3S_4Cp_3][Sn(CH_3)_3Cl_2]$ (Cp: C_5H_5).[27] There are no significant differences in Mo–S distances among the compounds listed in Table 2.

As for [**6**]PF$_6$·4CH$_2$Cl$_2$, statistical disorder was observed between two μS and one μO atoms. The μS and μO atoms were refined with a partial occupancy of 2/3 and 1/3, respectively. Only the two μS atoms and one μO atom are included in the ORTEP drawing of **6** for clarity. No statistical disorder was observed between two μS and one μO atoms in [**8**]PF$_6$·2.5CH$_2$Cl$_2$. The Mo–Mo distances (Mo–μS–Mo, 2.7557[1] Å; Mo–μO–Mo, 2.7225(6) Å) in **6** are slightly longer than those (Mo–μS–Mo, 2.705[18] Å; Mo–μO–Mo, 2.642(1) Å) in **2**.

The W–W, W–μS, and W–μ_3S distances in the analogous complexes having $W^{IV}{}_3S_4$ cores are listed in Table 3. The W–W distances (2.7891[2] Å) in **7** are longer by ca. 0.08 Å than those (2.708[5] Å) in **3**.[36] The elongation is probably due to the electron-donating property of the Tpe ligands. Cluster **7** has the longest W–W distances for the complexes that have a W_3S_4 core so far reported. The W–W distances (W–μS–W, 2.752[7] Å; W–μO–W, 2.6921(6) Å) in **8** are slightly longer than those (W–μS–W, 2.724[6] Å; W–μO–W, 2.620(1) Å) in $K_2[W_3OS_3(nta)_3]\cdot KCl\cdot 7H_2O$.[10]

Generally the M–M distances in M_3S_4 clusters are slightly longer than those in M_3OS_3 clusters (M = Mo or W).[7a]

Cluster **11** has a cubane-type Mo_3PdS_4 core and has a crystallographic C_3 symmetry, with the μ_3S, Pd, and Cl atoms on a threefold axis. All the molybdenum atoms bonded to the Tpe ligand. The Tpe ligand acts in a tridentate fashion and coordinated to the molybdenum atom through the two nitrogen atoms of the pyrazole rings and the one oxygen atom of the ethoxy group. The palladium atom bonded to the chloride anion.

Electronic Spectroscopy. The electronic spectra of [**5**]PF$_6$·3CH$_2$Cl$_2$ [λ_{max}/nm (ε/M^{-1} cm^{-1}) 625 (389)] and [**7**]PF$_6$·4CH$_2$Cl$_2$ [558 (641)] in acetonitrile together with those of **1** and **3** in 2 M Hpts (= *p*-toluenesulfonic acid) (Figure 6), and [**6**]PF$_6$·4CH$_2$Cl$_2$ [600 (304)] and [**8**]PF$_6$·2.5CH$_2$Cl$_2$ [485

Table 3. Comparison of W–W and W–S Distances (Å) in Incomplete Cubane-Type Compounds with $W^{IV}{}_3S_4$ Cores[a),b)]

Compound	W–W	W–μ_3S	W–μ_2S
$[W_3S_4(Tpe)_3]PF_6\cdot 4CH_2Cl_2$ ([**7**]$PF_6\cdot 4CH_2Cl_2$)	2.7891[2]	2.3648[15]	2.3074[16]
$[W_3S_4Cl_3(depe)_3]PF_6$[37]	2.776[3]	2.368[15]	2.305[17]
$(bpyH)_5[W_3S_4(NCS)_3]\cdot 3H_2O$[36]	2.764[4]	2.350[11]	2.306[11]
$[W_3S_4Cl_3(dmpe)_3]PF_6\cdot H_2O$[37]	2.755(1)	2.382(5)	2.308[14]
$[W_3S_4H_3(dmpe)_3]BPh_4$[37]	2.751[4]	2.354[2]	2.335[9]
$K_6[W_3S_4(HCO_2)_9]HCO_2\cdot 3H_2O$[38]	2.747[1]	2.350[4]	2.312[4]
$Na_2[W_3S_4(Hnta)_3]\cdot 5H_2O$[36]	2.738[15]	2.349[2]	2.305[9]
$\{[W_3S_4(H_2O)_7Cl_2](C_{36}H_{36}N_{24}O_{12})\}Cl_2\cdot 10H_2O$[39]	2.715[2]	2.340[7]	2.285[7]
$[W_3S_4(H_2O)_9](pts)_4\cdot 9H_2O$ ([**3**]$(pts)_4\cdot 9H_2O$)[36]	2.708[5]	2.338[8]	2.284[4]

a) Abbreviations: Hnta: $N(CH_2COO)_3H^{2-}$, dmpe: $Me_2P(CH_2)_2PMe_2$, depe: $Et_2P(CH_2)_2PEt_2$. b) Parentheses indicate esd of one value. The estimated deviation in brackets is calculated as being equal to $[\Sigma\Delta_i^2/n(n-1)]^{1/2}$, in which Δ_i is deviation of the ith (of n) value from the arithmetic mean of the n values.

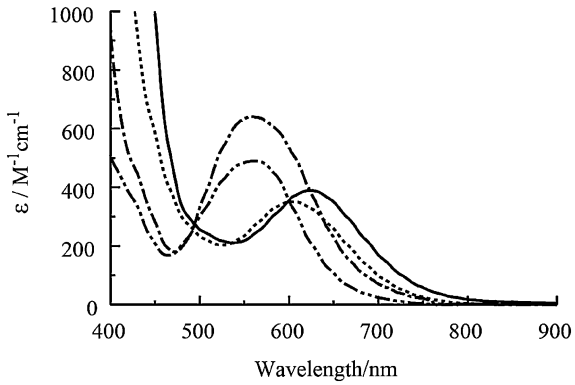

Figure 6. Electronic spectra of **5** (solid line) and **7** (dashed-dotted line) in MeCN and **1** (dashed line) and **3** (dashed-double dotted line) in 2 M Hpts.

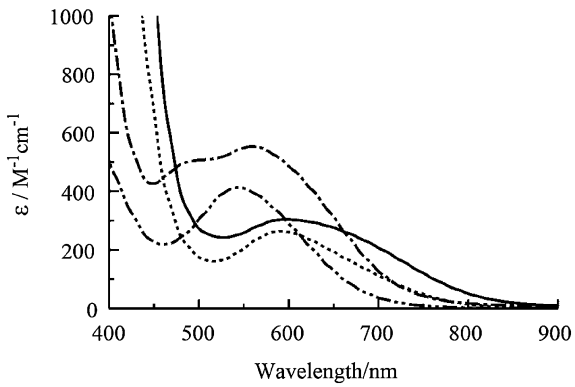

Figure 7. Electronic spectra of **6** (solid line) and **8** (dashed-dotted line) in MeCN and **2** (dashed line) and **4** (dashed-double dotted line) in 2 M Hpts.

(500), 558 (553)] together with those of **2** and **4** in 2 M Hpts (Figure 7) are shown in respective Figures.

The electronic spectra of [**11**]$\cdot 4.5CH_2Cl_2$ [465 (1863), 575(1606)] and [**5**]$PF_6\cdot 4CH_2Cl_2$ in dichloromethane are shown in Figure 8.

The characteristic peak position for **5** appeared at a longer wavelength of 625 nm than that of aqua cluster **1**. This observation is consistent with the fact that nine water molecules attached to molybdenum atoms were substituted with three of

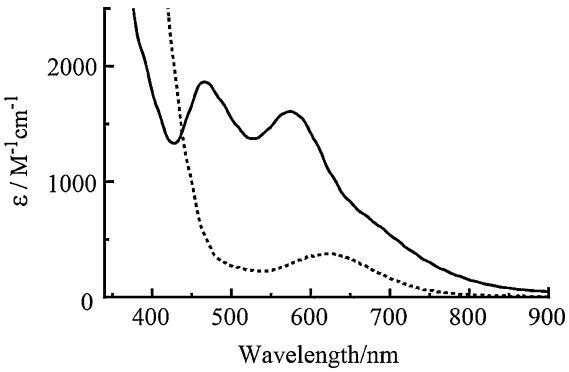

Figure 8. Electronic spectra of **11** (solid line) and **5** (dashed line) in CH_2Cl_2.

the electron-donating Tpe ligands. Similar spectral shifts were observed in the case of **9**.[7] The characteristic peak position at 558 nm for **7** in acetonitrile is close to that of aqua cluster **3** [560 (490)]: the ε value of **7** becomes 1.5 times larger than that of **3**. The reason for these results is uncertain at present.

The characteristic peak position for **6** appeared at a longer wavelength of 600 nm than that of aqua cluster **2** [588 (263)]. The spectrum of **6** shows a broad peak in the visible region, while that of **3** has a relatively sharper peak in the region. The spectrum of **8** [485 (500), 558 (553)], which is a tungsten analogue of **6**, shows two broad peaks in the visible region, while that of **2** has one peak in the region. These changes may be caused by the lowering of symmetry in **6** and **8** through the substitution of one μS with one μO.

The spectrum of molybdenum–palladium cluster **11** shows two characteristic peaks in the visible region. Upon the ligand exchange from aqua to Tpe, the peak position of the second absorption band of **11** shifts to longer wavelength by 16 nm. The first absorption band also slightly shifted to longer wavelength by 5 nm.

The acetonitrile solutions of [**5**]PF_6, [**6**]PF_6, [**7**]PF_6, and [**8**]PF_6, and dichloromethane solution of **11** are stable in air.

^{1}H NMR Spectroscopy. The ^{1}H NMR spectra of [**5**]$PF_6\cdot 3CH_2Cl_2$ (Spectrum A) and [**7**]$PF_6\cdot 4CH_2Cl_2$ (Spectrum B) in CD_3CN at 298 K are shown in Figure 9. The spectra of [**5**]$PF_6\cdot 3CH_2Cl_2$ and [**7**]$PF_6\cdot 4CH_2Cl_2$ are close to each other. The numbering of the hydrogen atom positions of the pyrazole

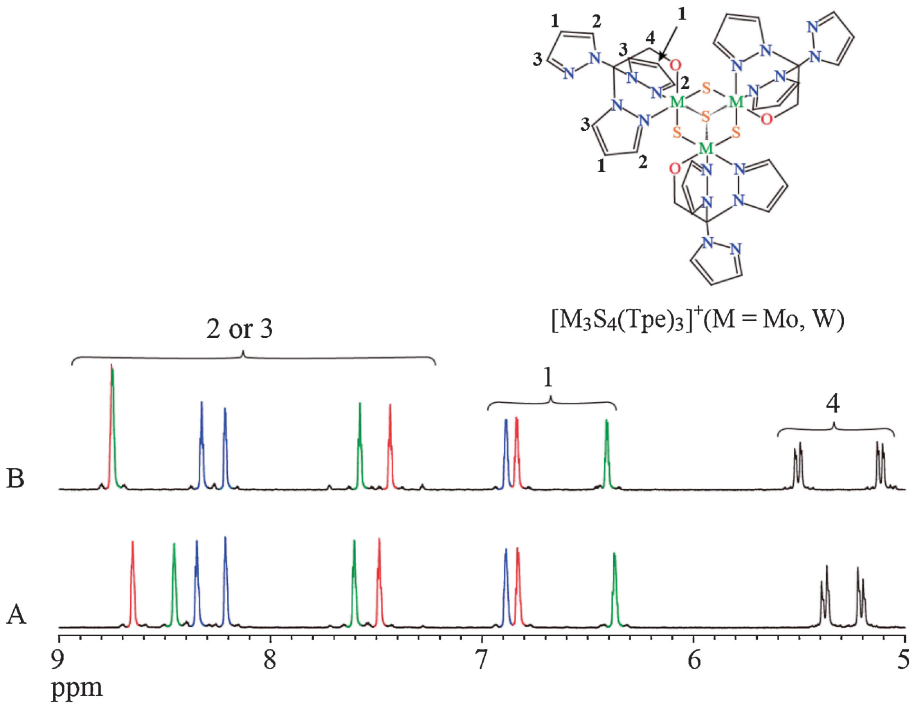

Figure 9. ^{1}H NMR spectra of [**5**]PF_6 (A) and [**7**]PF_6 (B) in CD_3CN (298 K, 400 MHz, CD_3CN = 2.00 ppm).

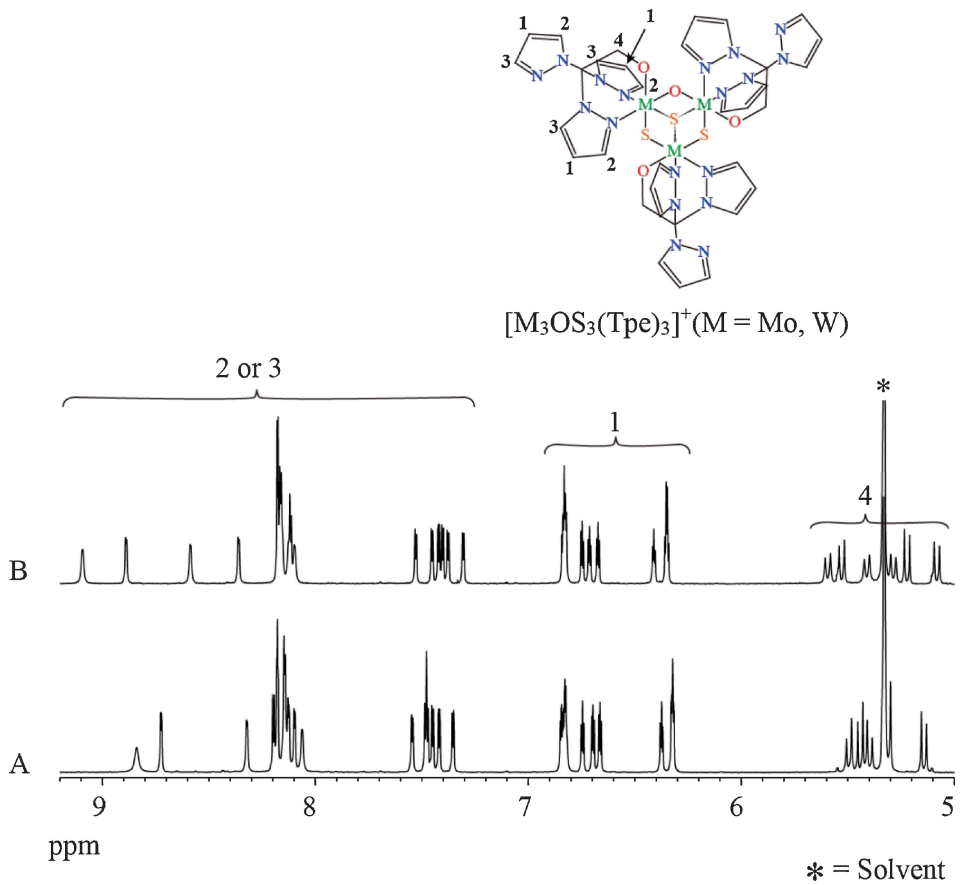

Figure 10. ^{1}H NMR spectra of [**6**]PF_6 (A) and [**8**]PF_6 (B) in CD_2Cl_2 (298 K, 400 MHz, CD_2Cl_2 = 5.33 ppm).

rings and methylene group of Tpe is indicated in the inset of Figure 9. Only eleven signals corresponding to three pyrazole rings and one methylene group in one Tpe were clearly observed at 298 K. It shows that both the clusters **5** and **7** have a threefold rotation axis in solution; that is to say, the three Tpe ligands are equivalent, and the three pyrazole rings in each Tpe ligand are in different environments. All the signals were assigned as shown in Figure 9. The triplets corresponding to three protons at 6.3–6.9 ppm were assigned to the protons belonging to the position 1. The doublets corresponding to six protons at 7.4–8.8 ppm were assigned to the protons belonging to the positions 2 and 3. The protons in the methylene group were observed as a doublet of doublets at 5.1–5.5 ppm. The signals with which correlations were seen by the HH correlation spectra of [**5**]$PF_6 \cdot 3CH_2Cl_2$ and [**7**]$PF_6 \cdot 4CH_2Cl_2$ are shown in the same colors, respectively.

^{1}H NMR spectra of [**6**]$PF_6 \cdot 4CH_2Cl_2$ (Spectrum A) and [**8**]$PF_6 \cdot 2.5CH_2Cl_2$ (Spectrum B) in CD_2Cl_2 at 298 K are shown in Figure 10. The spectra of [**6**]$PF_6 \cdot 4CH_2Cl_2$ and [**8**]$PF_6 \cdot 2.5CH_2Cl_2$ are similar to each other. The numbering of the hydrogen atom positions of the pyrazole rings and methylene group of Tpe is indicated in the inset of Figure 10. Obviously, **6** and **8** have no threefold rotation axis in contrast to **5** and **7**. The number of the independent proton signals originated from the three Tpe decreased from thirty-three to twenty-seven due to overlapping. All the signals were assigned as shown in Figure 10. The triplets corresponding to nine protons at 6.3–6.9 ppm were assigned to the protons belonging to the position 1. The doublets corresponding to eighteen protons at 7.3–8.8 ppm were assigned to the protons belonging to the positions 2 and 3. The protons in the methylene groups were clearly observed as a doublet of doublets at 5.1–5.6 ppm.

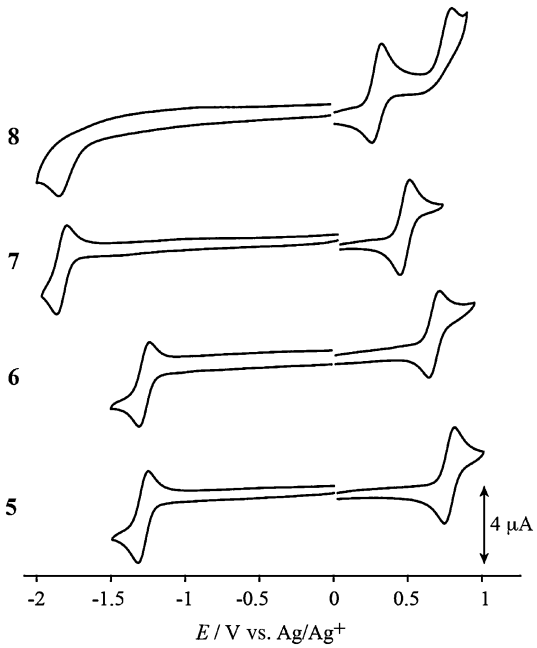

Figure 11. Cyclic voltammograms of **5** (0.5 mM), **6** (0.5 mM), **7** (0.5 mM), and **8** (0.5 mM) in MeCN containing 0.1 M *n*-Bu_4NPF_6 (scan rate: 100 mV s^{-1}).

Cyclic Voltammetry. The cyclic voltammograms of **5**, **6**, **7**, and **8** in acetonitrile are shown in Figure 11. The redox potentials of these clusters are listed in Table 4. All values are given vs. SHE.

The cyclic voltammograms of **5** and **7**, which have M_3S_4 (M = Mo and W) cores, show one reversible one-electron oxidation process and one reversible one-electron reduction process. The oxidation process corresponds to the change of the oxidation states of the molybdenum or tungsten atoms: M_3 (IV, IV, IV) to M_3 (V, IV, IV). The reduction process corresponds to the change of the oxidation states of the molybdenum or tungsten atoms: M_3 (IV, IV, IV) to M_3 (IV, IV, III).

The redox potentials of **5** is significantly lower than those of **9**. This observation may reflect the better electron-donating ability of the Tpe ligand to the Mo_3S_4 moiety relative to the Tp ligand.

The cyclic voltammogram of **6**, which has a Mo_3OS_3 core, shows one reversible one-electron oxidation process and one reversible one-electron reduction process. The oxidation process also corresponds to the change of the oxidation states of the molybdenum atoms: Mo_3 (IV, IV, IV) to Mo_3 (V, IV, IV). The reduction process also corresponds to the change of oxidation states of the molybdenum atoms; Mo_3 (IV, IV, IV) to Mo_3 (IV, IV, III). Only one example was reported of the observation of reversible one-electron oxidation processes of the cluster having Mo_3OS_3 core.[7]

In the case of **8**, which is a tungsten analogue of molybdenum cluster **6**, one reversible and one irreversible one-electron oxidation and one irreversible one-electron reduction were observed. The oxidation processes correspond to the change of the oxidation states of the tungsten atoms: W_3 (IV, IV, IV) to W_3 (V, IV, IV) and W_3 (V, IV, IV) to W_3 (V, V, IV). The reduction process corresponds to the change of the

Table 4. Half Wave Potential ($E_{1/2}$, V vs. SHE) Values of Clusters with Mo_3S_4, Mo_3OS_3, W_3S_4, and W_3OS_3 Cores

Cluster	$E_{1/2}$/V vs. SHE				
	IV III III/ III III III	IV IV III/ IV III III	IV IV IV/ IV IV III	V IV IV/ IV IV IV	V V IV/ V IV IV
$[Mo_3S_4(Tpe)_3]^+$ (**5**)	—	—	−0.96	+1.10	—
$[Mo_3S_4(Tp)_3]^+$ (**9**)[7a]	—	−1.38	−0.41	+1.62	—
$[Mo_3OS_3(Tpe)_3]^+$ (**6**)	—	—	−0.96	+1.00	—
$[Mo_3OS_3(Tp)_3]^+$ (**10**)[7a]	—	−1.59	−0.39	+1.55	—
$[W_3S_4(Tpe)_3]^+$ (**7**)	—	—	−1.54	+0.77	+1.38[a)]
$[W_3OS_3(Tpe)_3]^+$ (**8**)	—	—	−1.54[a)]	+0.61	+1.12[a)]

a) E_{pc} value.

Table 5. Binding Energies of the Clusters with Mo_3S_4, Mo_3PdS_4, Mo_3FeS_4, and Mo_3NiS_4 Cores

Compound	$Mo(3d_{3/2})$	$Mo(3d_{5/2})$	$Pd(3d_{3/2})$	$Pd(3d_{5/2})$
$[Mo_3S_4(Tpe)_3]PF_6$ ([**5**]PF_6)	232.6	229.4	—	—
$[Mo_3PdS_4Cl(Tpe)_3]$ ([**11**])	232.2	229.0	341.1	335.8
$[Mo_3S_4(Tp)_3]Cl$ ([**9**]Cl)	233.1	229.9	—	—
$[Mo_3PdS_4Cl(Tp)_3]$ ([**12**])	232.5	229.4	341.7	336.4
$[Mo_3S_4(H_2O)_9](pts)_4$ ([**1**]$(pts)_4$)[34]	233.6	230.7	—	—
$[Mo_3FeS_4(H_2O)_{10}](pts)_4$ ([**13**]$(pts)_4$)[17]	233.1	230.0	—	—
$[Mo_3NiS_4(H_2O)_{10}](pts)_4$ ([**14**]$(pts)_4$)[18]	233.3	230.3	—	—

oxidation states of the tungsten atoms: W_3 (IV, IV, IV) to W_3 (IV, IV, III). This is the first CV example of the observation of the cluster having W_3OS_3 core.

The oxidation potentials of **6** and **8** shifted to negative compared with those of **5** and **7**, respectively, that is, the substitution of O for S produces a negative shift in the potential of $Mo^{IV/V}$ oxidation. The influence of sulfur coordination on mononuclear molybdenum-centered electron transfer has been reported by Schultz and Uhrhammer,[40] where they reported that systematic substitution of S for O produces a positive shift in the potential of $Mo^{V/IV}$ reduction.

XPS Spectroscopy. The binding energy values of Mo $3d_{3/2}$, Mo $3d_{5/2}$, Pd $3d_{3/2}$, and Pd $3d_{5/2}$ obtained from the X-ray photoelectron spectroscopy measurement for [**5**]PF_6, [**9**]Cl, **11**, and **12** are listed in Table 5. For comparison, the values for [**1**]$(pts)_4$ (pts: *p*-toluenesulfonate), [**13**]$(pts)_4$, and [**14**]$(pts)_4$ are also listed in the table.

The formation reactions of **11** and **12** are reductive addition of palladium into Mo_3S_4 core (Scheme 2). Molybdenum atoms (Mo_3^{IV}) are reduced to Mo^{IV} Mo_2^{III} in the reaction. The palladium atom (Pd^0) is oxidized to Pd^{II}. In order to discuss the formal oxidation state of the palladium, the binding energy values of Pd $3d_{5/2}$ for **11** and **12** are compared with those of the mononuclear palladium compounds, $[Pd_2(dba)_3]$ (Pd $3d_{5/2}$, 336.4 eV), $[Pd(PPh)_4]$ (336.2), PdO (336.5), and PdS (336.3). Since there are no significant differences in the values between these compounds, it is difficult to assess the formal oxidation state of the palladium atom from this comparison. On the other hand, the binding energy values of Mo $3d_{3/2}$ and Mo $3d_{5/2}$ for **11** and **12** clearly show lower energy shifts than those of [**5**]PF_6 and [**9**]Cl, respectively. These energy shifts correspond to the formal oxidation states change of the molybdenum atoms from Mo_3^{IV} to Mo^{IV} Mo_2^{III}. These observations suggest that the reductive addition of Pd^0 occurred to give Mo^{IV} Mo_2^{III} Pd^{II} species. Similar observations were reported for the formation reactions of [**13**]$(pts)_4$[15,41] and [**14**]$(pts)_4$.[15]

The electron-donating abilities of the ligands are found to decrease in the order: Tpe > Tp > H_2O, because the binding energy values of Mo $3d_{3/2}$ and Mo $3d_{5/2}$ increases in the order of [**5**]PF_6 < [**9**]Cl < [**1**]$(pts)_4$.

Catalytic Reaction. The catalytic activity of $[Mo_3PdS_4Cl(Tacn)_3](PF_6)_3$ toward the intramolecular cyclization reaction of 4-pentynoic acid was reported.[42] In the presence of $[Mo_3PdS_4Cl(Tacn)_3](PF_6)_3$, 98% of 4-pentynoic acid was converted to γ-methylene-γ-butyrolactone and the turnover number of this reaction reached 100000 after 19 h at 40 °C. In the case of **11**, the same reaction requires 12 h under the same conditions. This result indicates that the catalytic activity of **11** is significantly increased by the introduction of the Tpe ligands.

Conclusion

$[Mo_3S_4(Tpe)_3]^+$ (**5**, Tpe = tris(pyrazolyl)ethanol), $[Mo_3OS_3(Tpe)_3]^+$ (**6**), $[W_3S_4(Tpe)_3]^+$ (**7**), and $[W_3OS_3(Tpe)_3]^+$ (**8**) have been successfully prepared. All these compounds are structurally characterized by X-ray structure analyses. All the molybdenum or tungsten atoms bonded to the Tpe ligand. Tpe ligand acts in a tridentate fashion and coordinated to the molybdenum or tungsten atom through the two nitrogen atoms of the pyrazole rings and the one oxygen atom of the ethoxy group. The cyclic voltammograms of **5**, **6**, and **7** show one reversible one-electron oxidation process and one reversible one-electron reduction process. In the case of **8**, one reversible and one irreversible one-electron oxidation processes and one irreversible one-electron reduction process were observed. The oxidation potentials of **6** and **8** shifted to negative compared with those of **5** and **7**, respectively, that is, the substitution of O for S produces a negative shift in the potential of $Mo^{IV/V}$ oxidation. All the compounds have also been characterized by ^1H NMR and electronic spectroscopy. $[Mo_3PdS_4Cl(Tpe)_3]$ (**11**) has been successfully isolated from the reaction of **5** with $[Pd_2(dba)_3]$ (dba: tris(dibenzylideneacetone)dipalladium). It became clear that the formal oxidation state of palladium atom in **11** is Pd(II). Cluster **11** functions as a catalyst for intramolecular cyclization of 4-pentynoic acid.

The authors acknowledge support by the MEXT-Supported Program for the Strategic Research Foundation at Private Universities, 2009–2013.

References

1 a) S. Trofimenko, *Scorpionates: The Coordination Chemistry of Polypyrazolylborate Ligands*, Imperial College Press, London, **1999**. b) C. Pettinari, *SCORPIONATES II: CHELATING BORATE LIGANDS*, Imperial College Press, London, **2008**.

2 a) O. Graziani, L. Toupet, M. Tilset, J.-R. Hamon, *Inorg. Chim. Acta* **2007**, *360*, 3083. b) L. M. R. Hill, M. K. Taylor, V. W. L. Ng, C. G. Young, *Inorg. Chem.* **2008**, *47*, 1044. c) N. Kitajima, K. Fujisawa, Y. Moro-oka, K. Toriumi, *J. Am. Chem. Soc.* **1989**, *111*, 8975. d) N. Kitajima, K. Fujisawa, C. Fujimoto, Y. Moro-oka, S. Hashimoto, T. Kitagawa, K. Toriumi, K. Tatsumi, A. Nakamura, *J. Am. Chem. Soc.* **1992**, *114*, 1277. e) J. A. Camerano, M. A. Casado, M. A. Ciriano, C. Tejel, L. A. Oro, *Chem.—Eur. J.* **2008**, *14*, 1897. f) A. S. Kumar, T. Tanase, M. Iida, *Langmuir* **2007**, *23*, 391.

3 a) F. A. Cotton, R. Llusar, W. Schwotzer, *Inorg. Chim. Acta* **1989**, *155*, 231. b) F. A. Cotton, Z. Dori, R. Llusar, W. Schwotzer, *Inorg. Chem.* **1986**, *25*, 3529.

4 H. Akashi, T. Shibahara, H. Kuroya, *Polyhedron* **1990**, *9*, 1671.

5 T. Shibahara, G. Sakane, S. Mochida, *J. Am. Chem. Soc.* **1993**, *115*, 10408.

6 S. Trofimenko, J. R. Long, T. Nappier, S. G. Shore, in *Inorganic Syntheses*, ed. by R. W. Parry, John Wiley & Sons, Inc., **1970**, Vol. 12, p. 99. doi:10.1002/9780470132432.ch18.

7 a) T. Yamauchi, H. Takagi, T. Shibahara, H. Akashi, *Inorg. Chem.* **2006**, *45*, 5429. b) T. Shibahara, H. Akashi, H. Kuroya, *J. Am. Chem. Soc.* **1986**, *108*, 1342. c) T. Yamauchi, H. Akashi, H. Takagi, T. Shibahara, *Abstract book of XXXVI International Conference on Coordination Chemistry P5.026*, Merida, Mexico, **2004**.

8 D. L. Reger, T. C. Grattan, *Synthesis* **2003**, 350.

9 T. Shibahara, K. Kohda, A. Ohtsuji, K. Yasuda, H. Kuroya, *J. Am. Chem. Soc.* **1986**, *108*, 2757.

10 T. Shibahara, A. Takeuchi, H. Kuroya, *Inorg. Chim. Acta* **1987**, *127*, L39.

11 T. Higashi, *ABSCOR*, Rigaku Corporation, Tokyo, Japan, **1995**.

12 G. M. Sheldrick, *SHELX97*, **1997**.

13 *Rigaku: CrystalStructure Ver. 3.8.2*, Rigaku Corporation, Tokyo, Japan, **2006**.

14 T. Shibahara, H. Akashi, M. Yamasaki, K. Hashimoto, *Chem. Lett.* **1991**, 689.

15 T. Shibahara, G. Sakane, Y. Naruse, K. Taya, H. Akashi, A. Ichimura, H. Adachi, *Bull. Chem. Soc. Jpn.* **1995**, *68*, 2769.

16 H. Akashi, T. Shibahara, *Inorg. Chim. Acta* **2000**, *300–302*, 572.

17 G. Sakane, H. Kawasaki, T. Oomori, M. Yamasaki, H. Adachi, T. Shibahara, *J. Cluster Sci.* **2002**, *13*, 75.

18 T. Shibahara, S. Kobayashi, N. Tsuji, G. Sakane, M. Fukuhara, *Inorg. Chem.* **1997**, *36*, 1702.

19 G. Sakane, H. Kawasaki, M. Yamasaki, H. Adachi, T. Shibahara, *Chem. Lett.* **1999**, 631.

20 G. Sakane, T. Shibahara, *Inorg. Chem.* **1993**, *32*, 777.

21 H. Akashi, T. Shibahara, *Inorg. Chem.* **1989**, *28*, 2906.

22 a) G. Sakane, K. Hashimoto, M. Takahashi, M. Takeda, T. Shibahara, *Inorg. Chem.* **1998**, *37*, 4231. b) T. Shibahara, K. Hashimoto, G. Sakane, *J. Inorg. Biochem.* **1991**, *43*, 280.

23 a) I. Takei, K. Suzuki, Y. Enta, K. Dohki, T. Suzuki, Y. Mizobe, M. Hidai, *Organometallics* **2003**, *22*, 1790. b) K. Herbst, P. Zanello, M. Corsini, N. D'Amelio, L. Dahlenburg, M. Brorson, *Inorg. Chem.* **2003**, *42*, 974. c) M. N. Sokolov, D. Villagra, A. M. El-Hendawy, C.-H. Kwak, M. R. J. Elsegood, W. Clegg, A. G. Sykes, *J. Chem. Soc., Dalton Trans.* **2001**, 2611.

24 a) G. Sakane, Y.-g. Yao, T. Shibahara, *Inorg. Chim. Acta* **1994**, *216*, 13. b) S.-F. Lu, Y. Peng, H.-J. Fan, Q.-J. Wu, Z.-X. Huang, J.-Q. Huang, *J. Cluster Sci.* **2002**, *13*, 15. c) Y. Qin, L. Wu, Z. Li, Y. Kang, Y. Tang, Y. Yao, *Chem. Lett.* **2000**, 950.

25 G. Sakane, T. Shibahara, H. Adachi, *J. Cluster Sci.* **1995**, *6*, 503.

26 I. Takei, K. Suzuki, Y. Enta, K. Dohki, T. Suzuki, Y. Mizobe, M. Hidai, *Organometallics* **2003**, *22*, 1790.

27 P. J. Vergamini, H. Vahrenkamp, L. F. Dahl, *J. Am. Chem. Soc.* **1971**, *93*, 6327.

28 T. Saito, N. Yamamoto, T. Yamagata, H. Imoto, *Chem. Lett.* **1987**, 2025.

29 T. R. Halbert, K. McGauley, W.-H. Pan, R. S. Czernuszewicz, E. I. Stiefel, *J. Am. Chem. Soc.* **1984**, *106*, 1849.

30 N. C. Howlader, G. P. Haight, T. W. Hambley, Jr., G. A. Lawrance, K. M. Rahmoeller, M. R. Snow, *Aust. J. Chem.* **1983**, *36*, 377.

31 a) J. Q. Huang, J. L. Huang, M. Y. Shang, S. F. Lu, X. T. Lin, Y. H. Lin, M. D. Huang, H. H. Zhuang, J. X. Lu, *Pure Appl. Chem.* **1988**, *60*, 1185. b) X.-T. Lin, Y.-H. Lin, J.-L. Huang, J.-Q. Huang, *Kexue Tongbao* **1987**, *32*, 810.

32 M. Yamasaki, T. Shibahara, *Anal. Sci.* **1992**, *8*, 727.

33 T. Shibahara, H. Kuroya, *Polyhedron* **1986**, *5*, 357.

34 M.-D. Huang, S.-F. Lu, J.-Q. Huang, J.-L. Huang, *Acta Chimi. Sin.* **1989**, *47*, 121.

35 a) F. A. Cotton, R. Llusar, *Polyhedron* **1987**, *6*, 1741. b) F. A. Cotton, Z. Dori, R. Llusar, W. Schwotzer, *J. Am. Chem. Soc.* **1985**, *107*, 6734.

36 T. Shibahara, A. Takeuchi, A. Ohtsuji, K. Kohda, H. Kuroya, *Inorg. Chim. Acta* **1987**, *127*, L45.

37 F. A. Cotton, R. Llusar, C. T. Eagle, *J. Am. Chem. Soc.* **1989**, *111*, 4332.

38 M. Brorson, A. Hazell, C. J. H. Jacobsen, I. Schmidt, J. Villadsen, *Inorg. Chem.* **2000**, *39*, 1346.

39 V. P. Fedin, A. V. Virovets, M. N. Sokolov, D. N. Dybtsev, O. A. Gerasko, W. Clegg, *Inorg. Chem.* **2000**, *39*, 2227.

40 D. Uhrhammer, F. A. Schultz, *Inorg. Chem.* **2004**, *43*, 7389.

41 M. Katada, H. Akashi, T. Shibahara, H. Sano, *J. Radioanal. Nucl. Chem.* **1990**, *145*, 143.

42 T. Wakabayashi, Y. Ishii, K. Ishikawa, M. Hidai, *Angew. Chem., Int. Ed. Engl.* **1996**, *35*, 2123.